Environ. Sci. Technol. **2006**, *40,* 4696−4702

In Situ Redox Flexibility of Fe^{II-III} Oxyhydroxycarbonate Green Rust and Fougerite

CHRISTIAN RUBY, CHANDAN UPADHYAY,
ANTOINE GÉHIN,
GEORGES ONA-NGUEMA, AND
JEAN-MARIE R. GÉNIN*

Laboratoire de Chimie Physique et Microbiologie pour l'Environnement, UMR 7564 CNRS−Université Henri Poincaré-Nancy 1, Equipe Microbiologie, Physique et Chimie Douce and Département Matériaux et Structures, ESSTIN, 405 rue de Vandoeuvre, F-54600 Villers-lès-Nancy, France

Bacterial activity is commonly thought to be directly responsible for denitrification in soils and groundwater. However, nitrate reduction in low organic sediments occurs abiotically by Fe^{II} ions within the fougerite mineral (IMA 2003-057), giving the bluish-green color of gleysols. Fougerite, the mineral counterpart of Fe^{II-III} oxyhydroxycarbonate, $Fe^{II}_{6(1-x)}Fe^{III}_{6x}O_{12}H_{2(7-3x)}CO_3$, provides a unique in situ redox flexibility, which can adapt $x = \{[Fe^{III}]/[Fe_{total}]\}$ between 1/3 and 2/3 as shown using Mössbauer spectroscopy. Chemical potential and E_h−pH diagrams for this system were determined from electrode potential monitored during deprotonation of hydroxycarbonate $Fe^{II}_4Fe^{III}_2(OH)_{12}CO_3$ to assess the possibility of reducing pollutants in the field. Bioreduction of ferric oxyhydroxides in anoxic groundwater yields dissolved Fe^{II}, whereas HCO_3^- anions produced from organic matter are incorporated into fougerite layered double oxyhydroxide structure. Thus, fougerite is the solid-state redox mediator acting as electron shuttle that helps bacterial activity for reducing nitrate by coupling dissimilatory Fe^{III} reduction and oxidation of Fe^{II} with reduction of NO_3^-. It is proposed that this system could be used in the remediation of soils and nitrified waters.

Introduction

Preservation and/or remediation of groundwater are of utmost importance because human activities need ever-more water resources. Industry and agriculture sometimes threaten these resources, and remediation often becomes necessary. Nitrate is a major nonpoint source pollutant responsible for many dangers, e.g., blue baby syndrome, algae proliferation, etc. Microbial denitrification is commonly accepted as the main nitrate-reducing process in sediments with high bioavailable organic matter content, where nitrate acts as electron acceptor for respiration (*1*−*4*). The capacity for microbial denitrification is limited in sediments poor in organic matter, where, however, abiotic denitrification becomes the major factor (*5*−*7*). Thus, reduced Fe^{II} iron in various minerals belongs to the pool of reductants that are active for abiotic nitrate reduction.

Hydromorphic soils have typical depth profiles (*8*) presenting (*i*) an organic top cover of a few tens of cm thick comprising humic substances, (*ii*) beneath, an upper mineral layer getting progressively ochrous with scattered orange dots from top to bottom and that can reach meters in depth at the water level, and (*iii*) underneath, the gley, which is pale bluish-green resembling celadon porcelain and looking homogeneous and ductile. The color change from ochrous to bluish-green has been associated long ago with the change from ferric to ferrous iron, creating a redox front that follows the water level (*6*−*9*). The mineral incorporating Fe^{II} cations remained a mystery until ^{57}Fe Mössbauer spectra showed that it was an Fe^{II-III} green rust (GR) as encountered in the corrosion of iron base materials, named fougerite (IMA 2003-057) because samples were first extracted from the forest in Fougères (Brittany-France) (*10*−*12*).

Such Fe^{II-III} hydroxysalts belonging to the layered double hydroxide (LDH) family consist of $[Fe^{II}_{(1-x)}Fe^{III}_x(OH)_2]^{x+}$ brucite-like layers and interlayers, $[(x/n)A^{n-}\cdot(mx/n)H_2O]^{x-}$, containing A^{n-} anions and water molecules balancing the cation layer charge (*12, 13*). Although spectra of fougerite display a quadrupole doublet with large splitting ($\Delta \approx 3$ mm s^{-1}) attributed to Fe^{II} cations and a doublet with small splitting ($\Delta \approx 0.4$ mm s^{-1}) attributed to Fe^{III}, doublet intensities did not match those of any known synthetic GR, which, e.g., incorporates Cl^-, SO_4^{2-}, or CO_3^{2-} anions (*12*). This creates ambiguity for interpreting data and an old ferrosic hydroxide $Fe(OH)_{(2+x)}$ assumption (*14*) was offered as plausible explanation (*12, 15*), but X-ray diffraction (XRD) used in these studies was inappropriate for identifying a mineral in minority. Moreover, its reactivity and lability made analysis difficult. ^{57}Fe Mössbauer spectroscopy delivers the most reliable information concerning ratio $x = \{[Fe^{III}]/[Fe_{total}]\}$. As for all LDH, trivalent cations are distributed in a hexagonal pavement surrounded by six divalent cations due to electrostatic repulsion (*16*). Therefore, x cannot exceed (1/3), and GRs that have been synthesized, either by oxidizing $Fe(OH)_2$ in air in the presence of various anions or by coprecipitating a mixture of Fe^{II} and Fe^{III} salts, have an x ratio between (1/4) and (1/3) (*17*−*20*). In contrast, this mineral, once extracted from soils and sediments, has an x ratio always exceeding (1/3) that varies continuously up to (2/3) within the redox front depending on the depth of extraction (*6, 11, 12, 21*). Deprotonation of OH^- ions at the apexes of the octahedrons surrounding iron cations was recently pointed out (*22*), and orange-brown "ferric green rust" $GR(CO_3^{2-})^*$ was obtained at $x = 1$ by violent oxidation of $GR(CO_3^{2-})$ with H_2O_2 or aerial oxidation of carefully dried $GR(CO_3^{2-})$.

This article aims at demonstrating that deprotonation takes place in situ and hydroxycarbonate $GR(CO_3^{2-})$ continuously transforms into oxyhydroxycarbonate $GR^*(x)$, $Fe^{II}_{6(1-x)}\,Fe^{III}_{6x}\,O_{12}\,H_{2(7-3x)}\,CO_3$, characterized by an x value in agreement with Mössbauer spectra of natural samples. Chemical potentials are determined for each composition x, and E_h−pH diagrams are drawn showing whether certain pollutants could be reduced by this GR. Redox flexibility of fougerite, limited to $x \in [(1/3), (2/3)]$ (*6, 11, 12, 21*), which forms in anoxic waterlogged soils by bioreduction likely participates to, e.g., nitrate reduction. This becomes a clue for designing large-scale remediation strategies for polluted aquifers by copying and enhancing the way Nature does it.

Experimental Section

Preparation of Stoichiometric $GR(CO_3^{2-})$. Stoichiometric $GR(CO_3^{2-})$ at $x = 1/3$, $Fe^{II}_4Fe^{III}_2(OH)_{12}CO_3$, was obtained by coprecipitating Fe^{II} and Fe^{III} ions in carbonate-containing solution. It was necessary to first obtain a precipitate using

---

* Corresponding author phone: +33(0)383685236; fax: +33(0) 383275444; e-mail: genin@lcpme.cnrs-nancy.fr.

10.1021/es0606834 CCC: $33.50

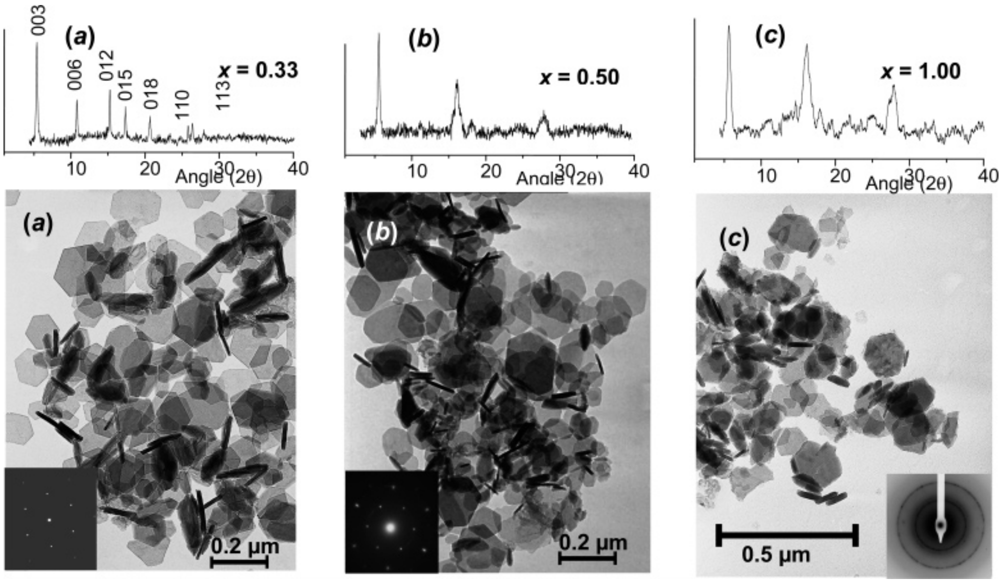

FIGURE 1. Transmission electron micrographs and X-ray diffraction patterns of Fe^{II-III} (oxy)hydroxycarbonate. (a) $GR(CO_3^{2-})$ obtained by coprecipitation of Fe^{II} and Fe^{III} species at $x = 0.33$. (b) $GR(CO_3^{2-})^*$ at $x = 0.50$ obtained by partial deprotonation with H_2O_2. (c) Total deprotonation obtained by fast oxidation of $GR(CO_3^{2-})$ with H_2O_2 leading to the fully ferric $GR(CO_3^{2-})^*$ at $x = 1$.

soluble species (e.g., SO_4^{2-}) before adding Na_2CO_3 since carbonate salts were not soluble. Such procedures were previously documented for $GR(SO_4^{2-})$ (*23*) and $GR(CO_3^{2-})$ (*24*). $FeSO_4{\cdot}7H_2O$ and $Fe_2(SO_4)_3{\cdot}5H_2O$ salts were dissolved in demineralized water ([Fe] = 0.4 M) with ferric molar fraction $x = \{n(Fe^{III})/n(Fe_{total})\}$ fixed at (1/3). Few Na_2HPO_4 ($[PO_4^{3-}] = 2 \times 10^{-2}$ M) was dissolved in the initial mixture to stabilize $GR(CO_3^{2-})$ (*24*). Sodium carbonate Na_2CO_3 (0.47 M) was added to a 1 M NaOH solution with molar ratio $R = \{n(NaOH)/n(Fe_{total})\}$ fixed at 2. Then, the basic solution was mixed into the initial Fe^{II-III} solution and the resulting product was stored in a glass flask sheltered from the air.

Preparation of Oxyhydroxycarbonate with Variable Composition. Two methods for synthesizing fully ferric green rust $GR(CO_3^{2-})^*$ could have been chosen: (*i*) fast oxidation of $GR(CO_3^{2-})$ in an aqueous medium by hydrogen peroxide solution; or (*ii*) oxidation in the air of a previously dried $GR(CO_3^{2-})$ sample. The first method was chosen for providing a controlled amount of oxidant. Thus, $GR(CO_3^{2-})$ was first synthesized as explained previously such that the suspension contained well-crystallized hexagonal plates of about 200 nm diameter (Figure 1a). A 10.14 M H_2O_2 solution was then added to the $GR(CO_3^{2-})$ suspension at a targeted molar ratio $\{n(H_2O_2)/n(Fe_{total})\}$. For ratios larger than (1/3), the color changes from bluish-green to brown-orange and all Fe^{II} ions are oxidized to yield “fully ferric green rust”:

$$Fe^{II}_4\,Fe^{III}_2\,(OH)_{12}\,CO_3 + 2\,H_2O_2 \rightarrow Fe^{III}_6\,O_{12}\,H_8\,CO_3 + 4H_2O \quad (1)$$

In contrast, for ratio smaller than (1/3), an adequate amount of H_2O_2 solution, i.e., $\{n(H_2O_2)/n(Fe_{total})\} = (3x - 1)/6$, is added with a micropipet so as to reach any x value:

$$Fe^{II}_4\,Fe^{III}_2(OH)_{12}CO_3 + (3x - 1)H_2O_2 \rightarrow Fe^{II}_{6(1-x)}Fe^{III}_{6x}O_{12}H_{2(7-3x)}CO_3 + 2(3x - 1)H_2O \quad (2)$$

Values of x were targeted evenly between (1/3) and 1 at (1/2), (2/3), and (5/6).

Continuous deprotonation was monitored by recording electrode potential and pH with time whereas hydrogen peroxide was poured at a rate of about 0.7 mL min^{-1} in the initial $GR(CO_3^{2-})$ with a peristaltic pump. E_h values, referred to standard hydrogen electrode, allowed determining the chemical potential of oxyhydroxycarbonate as function of x.

Characterization Methods. After a few minutes of settling, solutions were filtered and dried in a glovebox filled with nitrogen. X-ray diffraction (XRD) patterns (Mo Kα_1, $\lambda = 0.07093$ nm) were measured on fully dried powder samples introduced in 1 mm glass capillaries that were sealed to avoid any oxidation during analysis. Transmission electron micrographs (TEM) were obtained using a Jeol microscope operating at 200 kV, and samples were prepared by depositing a drop of dispersed suspension on a copper grid under 10^{-8} mbar vacuum. Mössbauer spectra were recorded at 78 K using a constant acceleration spectrometer with ^{57}Co source in Rh matrix. Absorbers were prepared in a glovebox from finely ground powder introduced rapidly in the cryostat under helium. Spectra were fitted to Lorentzian shape lines, or to Voigt profile, the convolution of Gaussian distribution with Lorentzian line. Isomer-shifts δ refer to α-Fe spectrum at room temperature.

Results

Fe^{II-III} Oxyhydroxycarbonate Characterization. Samples prepared at $x = 0.50$ and $x = 1$ were hexagonal platy crystals similar to those of initial $GR(CO_3^{2-})$ (Figure 1b and c). XRD patterns confirmed that the main crystallographic features were maintained: e.g., the most intense line of $GR(CO_3^{2-})^*$ corresponded to (003) of $GR(CO_3^{2-})$, but lines were broadened with small contraction of the unit cell, ~5% (Figure 1b and c). The oxidation process preserved the CO_3^{2-} interlayers, and the quantity of CO_3^{2-} remained constant while rising x up to 1 (*25*).

Mössbauer spectrum of initial $GR(CO_3^{2-})$ fitted with Lorentzian lines displayed two ferrous doublets D_1 and D_2 with large splitting Δ of 2.92 and 2.63 mm s^{-1} and one ferric D_3 with small Δ of 0.47 mm s^{-1} in (1/2):(1/6):(1/3) intensity ratio (Figure 2a and b, Table 1). Isomer shifts δ of 1.25 mm s^{-1} for D_1 and D_2 and 0.48 mm s^{-1} for D_3 characterize low spin Fe^{II} and Fe^{III} states. Moreover, D_1 and D_2 are due to Fe^{II} far from any CO_3^{2-} and for Fe^{II} in register with the central C of CO_3^{2-}, respectively (*22*).

When $GR(CO_3^{2-})$ was oxidized by adding appropriate amounts of H_2O_2, obtained x values were 0.50, 0.63, 0.78, and

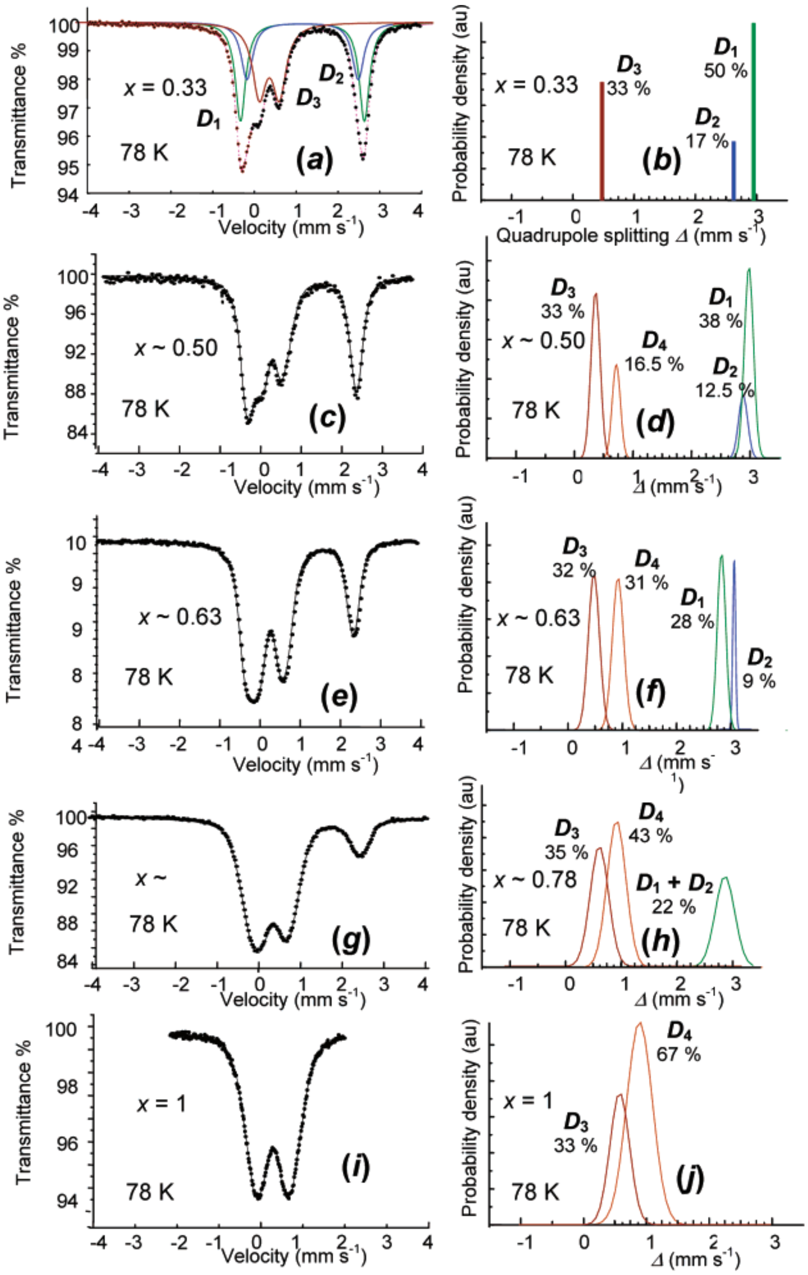

FIGURE 2. Mössbauer spectra measured at 78 K of (oxy)hydroxycarbonate GR(CO_3^{2-})*, which is obtained by fast oxidation with controlled amounts of H_2O_2 giving $x = \{[Fe^{III}]/[Fe_{total}]\} = 0.33, 0.50, 0.63, 0.78, 1$ and Gaussian distributions of quadrupole splitting Δ (Table 1).

1 for targets at (1/2), (2/3), (5/6), and 1. Spectra measured at 78 K were fitted by Voigt profile, giving mean values $\langle\Delta\rangle$ and standard deviations $\langle\delta\Delta\rangle$ of quadrupole splitting (Figure 2c−j, Table 1). A new ferric component D_4 appeared, whereas ferrous doublets D_1 and D_2 decreased with increasing x ratio. Components D_1 and D_2 remained in the 3:1 ratio, a feature that characterizes CO_3^{2-}anions by comparison to other GRs in which different anions are intercalated, e.g., Cl^- or SO_4^{2-} (*22*). Deprotonation equally affected both types of Fe^{II} ions. GR(CO_3^{2-})*, $Fe^{II}_{6(1-x)}Fe^{III}_{6}O_{12}H_{2(7-3x)}CO_3$ oxyhydroxycarbonate, exists continuously in the [(1/3)−1] range of x giving four doublets in Mössbauer spectra, D_1 and D_2 for Fe^{II} state and D_3 and D_4 for Fe^{III} state with relative abundances of $(3/4)(1-x)$, $(1/4)(1-x)$, 0.33, and $(x-0.33)$, respectively. Isomer shift δ values are identical for D_1 and D_2 doublets around 1.2 mm s^{-1}, and for D_3 and D_4, between 0.47 and 0.49 mm s^{-1}. Quadrupole splitting Δ values vary more widely due to significant changes in electric field gradient, and in particular for Fe^{III} cations, those of D_4 are twice those of D_3 due to distortion of octahedral sites resulting from a mixture of OH^- and O^{2-} ions at the octahedron apices.

Fe^{II-III} Oxyhydroxycarbonate Chemical Potential. E_h electrode potential variations (V_{SHE}) were recorded while adding H_2O_2 progressively to initial GR(CO_3^{2-}) precipitate with a peristaltic pump at constant rate in terms of experimental parameter $\{[2n(H_2O_2)/n(Fe_{total})] + (1/3)\}$ (Table 2, Figure 3a). E_h increased continuously from about −0.2 to +0.25 V during experiment, staying constant after complete oxidation was reached between 27 and 35 min from the start. Abscissa is converted in $x = \{[Fe^{III}]/[Fe_{total}]\} \in [(1/3)-1]$; pH stayed constant at 10 ± 0.2.

Half-reaction corresponding to reaction 1 written for reduction if GR is oxidized to ferric GR* is

$$Fe^{III}{}_6O_{12}H_8CO_3 + 4H^+ + 4e^- \rightarrow Fe^{II}{}_4Fe^{III}{}_2(OH)_{12}CO_3 \quad (3)$$

TABLE 1. Hyperfine Parameters of $GR(CO_3^{2-})^*$ for $x = [Fe^{III}]/[Fe_{Total}] \in [(1/3)-1]$[a]

	quadrupole doublets	δ (mm s^{-1})	$\langle\Delta\rangle$ (mm s^{-1})	$\langle\delta\Delta\rangle$ (mm s^{-1})	*RA* (%)
			$x = 0.33$		
Fe^{II}	D_1	1.25	2.92	0	50
	D_2	1.25	2.63	0	17
Fe^{III}	D_3	0.48	0.47	0	33
			$x \approx 0.50$		
Fe^{II}	D_1	1.21	2.98	0.14	38
	D_2	1.21	2.72	0.16	12.5
Fe^{III}	D_3	0.49	0.40	0.15	33
	D_4	0.49	0.70	0.28	16.5
			$x \approx 0.63$		
Fe^{II}	D_1	1.24	2.80	0.15	28
	D_2	1.24	3.05	0.05	9
Fe^{III}	D_3	0.48	0.49	0.20	32
	D_4	0.48	0.90	0.21	31
			$x \approx 0.78$		
Fe^{II}	$D_1 + D_2$	1.21	2.89	0.31	22
Fe^{III}	D_3	0.47	0.45	0.32	35
	D_4	0.47	0.95	0.34	43
			$x = 1$		
Fe^{III}	D_3	0.47	0.60	0.30	33
	D_4	0.47	0.88	0.41	67

[a] Values of x experimentally obtained are approximately 0.50, 0.63, and 0.78, and precisely 0.33 and 1. Spectra are measured at 78 K (Figure 2) and fitting uses a Voigt profile. δ : isomer shift in mm s^{-1} (reference is α-iron at ambient); $\langle\Delta\rangle$: mean value of quadrupole splitting in mm s^{-1}; and $\langle\delta\Delta\rangle$: its standard deviation; RA (%): relative area

and half-reaction corresponding to reaction 2 going from GR(1/3) to GR*(x) is

$$\mathrm{Fe^{II}}_{6(1-x)}\mathrm{Fe^{III}}_{6x}\mathrm{O_{12}H_{2(7-3x)}CO_3} + 2(3x-1)\ \mathrm{H^+} + 2(3x-1)\ \mathrm{e^-} \rightarrow \mathrm{Fe^{II}}_4\mathrm{Fe^{III}}_2\mathrm{(OH)_{12}CO_3} \quad (4)$$

Measurement of electrode potential E_h proceeds continuously vs x during deprotonation. We assumed equilibrium between GR*(x) and GR*(x + dx) during the increase of E_h if dx is the deprotonation increment leading to half-reaction

$$\mathrm{Fe^{II}}_{6[1-(x+dx)]}\mathrm{Fe^{III}}_{6(x+dx)}\mathrm{O_{12}H_{2[7-3(x+dx)]}CO_3} + (6 \times dx)\mathrm{H^+} + (6 \times dx)\mathrm{e^-} \rightarrow \mathrm{Fe^{II}}_{6(1-x)}\mathrm{Fe^{III}}_{6x}\mathrm{O_{12}H_{2(7-3x)}CO_3} \quad (5)$$

That is to summarize per iron atom

$$\mathrm{GR^*}(x+dx) + dx\ \mathrm{H^+} + dx\ \mathrm{e^-} \rightarrow \mathrm{GR^*}(x) \quad (6)$$

Because the numbers of electrons and protons are equal, Nernst's law becomes

$$E_h(x) = E^\circ(x) - 0.0591\mathrm{pH} \quad (7)$$

where E° is the standard counterpart of measured electrode potential E_h.

Chemical potentials are related at equilibrium in the standard conditions to $E^\circ(x)$

$$E^\circ(x) = \{\mu^\circ[\mathrm{GR^*}(x + dx)] - \mu^\circ[\mathrm{GR^*}(x)]\}/[dx \times \boldsymbol{F}] \quad (8)$$

where $\boldsymbol{F}$ is a Faraday and dx is the number of exchanged electrons.

$$\text{For } dx \rightarrow 0:\ \{\partial\mu^\circ[\mathrm{GR^*}(x)]/\partial x\} = E^\circ(x) \times \boldsymbol{F} = \{E_h(x) + 0.0591\mathrm{pH}\} \times \boldsymbol{F} \quad (9)$$

TABLE 2. Electrode Potential E_h Measured during the Deprotonation of $GR(CO_3^{2-})$ vs $x = \{[Fe^{III}]/[Fe_{total}]\}$ and Computed Chemical Potential $\mu^\circ[GR^*(x)]$ [eq 11]

x	E_h (V_{SHE})	$\mu^\circ[GR^*(x)]$ (kJ mole^{-1})	x	E_h (V_{SHE})	$\mu^\circ[GR^*(x)]$ (kJ mole^{-1})
0.33	**−0.2102**	**−600.27**	0.66	0.1061	−582.11
0.34	−0.2085	−599.91	**0.67**	**0.1063**	**−581.46**
0.35	−0.1950	−599.55	0.68	0.1063	−580.81
0.36	−0.1637	−599.17	0.69	0.1158	−580.03
0.37	−0.1550	−598.76	0.70	0.1179	−579.37
0.38	−0.1446	−598.35	0.71	0.1183	−578.71
0.39	−0.1373	−597.93	0.72	0.1182	−578.04
0.40	−0.1116	−597.48	0.73	0.1198	−577.38
0.41	−0.0936	−597.03	0.74	0.1201	−576.59
0.42	**−0.0858**	**−596.56**	**0.75**	**0.1240**	**−575.92**
0.43	−0.0735	−596.08	0.76	0.1238	−575.26
0.44	−0.0586	−595.59	0.77	0.1296	−574.59
0.45	−0.0434	−595.08	0.78	0.1323	−573.92
0.46	−0.0351	−594.57	0.79	0.1326	−573.24
0.47	−0.0199	−594.04	0.80	0.1357	−572.43
0.48	−0.0121	−593.50	0.81	0.1378	−571.75
0.49	−0.0055	−592.85	0.82	0.1413	−571.07
0.50	**0.0124**	**−592.29**	**0.83**	**0.1434**	**−570.39**
0.51	0.0224	−591.72	0.84	0.1470	−569.70
0.52	0.0251	−591.15	0.85	0.1511	−568.87
0.53	0.0307	−590.58	0.86	0.1533	−568.18
0.54	0.0386	−589.87	0.87	0.1591	−567.49
0.55	0.0484	−589.28	0.88	0.1605	−566.79
0.56	0.0548	−588.68	0.89	0.1652	−566.08
0.57	0.0622	−588.07	0.90	0.1721	−565.38
0.58	**0.0768**	**−587.33**	0.91	0.1757	−564.52
0.59	0.0779	−586.71	**0.92**	**0.1835**	**−563.80**
0.60	0.0819	−586.09	0.93	0.1934	−563.08
0.61	0.0861	−585.48	0.94	0.2029	−562.34
0.62	0.0895	−584.82	0.95	0.2125	−561.59
0.63	0.0968	−584.18	0.96	0.2255	−560.84
0.64	0.1060	−583.41	0.97	0.2429	−559.91
0.65	0.1067	−582.76	0.98	0.2564	−559.13
0.66	0.1061	−582.11	0.99	0.2672	−558.33
0.67	**0.1063**	**−581.46**	**1.00**	**0.2720**	**−557.53**

Integrating from (1/3) to x, i.e., going from GR(1/3) to GR*(x) one obtains

$$\{\mu^\circ[\mathrm{GR^*}(x)] - \mu^\circ[\mathrm{GR}(1/3)]\} = \boldsymbol{F} \times \int E^\circ(x)dx = \boldsymbol{F} \times \{\int E_h(x)dx + \int 0.0591\mathrm{pH} \times dx\} \quad (10)$$

Finally, the standard chemical potential μ°[GR*(x)] of deprotonated GR*(x) is computed from the measured electrode potential $E_h(x)$ with solution buffered at pH around 10

$$\mu^\circ[\mathrm{GR^*}(x)] = \mu^\circ[\mathrm{GR}(1/3)] + \boldsymbol{F} \times \{\int E_h(x)dx + 0.0591\mathrm{pH} \times (x - 0.33)\} \quad (11)$$

From experimental measurements of $E_h(x)$ (Figure 3a), chemical potentials μ°[GR*(x)] are computed using eq 11 (Table 2, Figure 3b). Raw data for $E_h(x)$ (Table 2, Figure 3a) display two domains: from x = (1/3) to (2/3), [AB], curvature is negative whereas from (2/3) to 1, [BC], it is positive. This originates from long range ordering when Fe^{III} ions progressively replace Fe^{II}. Approximate values of μ°[GR*(x)] expressed in kJ mole^{-1} are μ°[GR*(x)] = ($-618 + 54x$) kJ mole^{-1} in range [(1/3)−(2/3)], [AB], and μ°[GR*(x)] = ($-632 + 75x$) kJ mole^{-1} in range [(2/3)−1], [BC].

Discussion

Fe^{II-III} Oxyhydroxycarbonate E_h−pH Diagrams. Having the chemical potentials allows drawing E_h−pH diagrams for reactions involving GR*(x) by in situ deprotonation (Figure

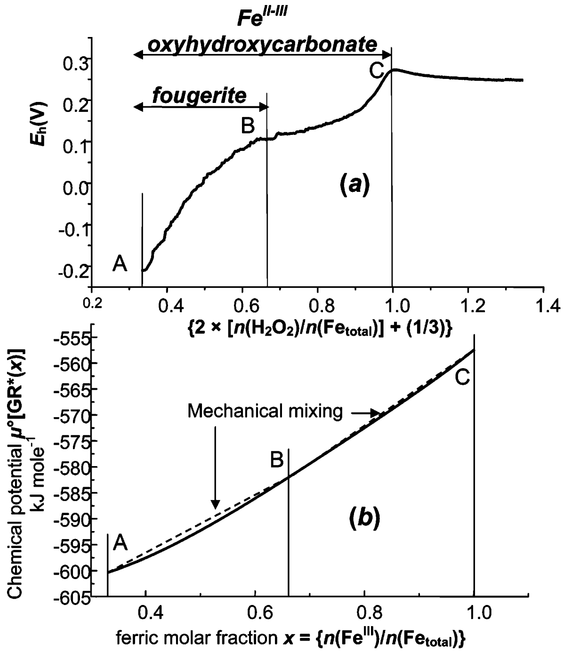

FIGURE 3. (a) Electrode potential E_h when adding H_2O_2 progressively to a $GR(CO_3^{2-})$ suspension leading to $GR^*(x)$ by deprotonation (values in Table 2); (b) chemical potential $\mu°[GR^*(x)]$ vs $x = \{[Fe^{III}]/[Fe_{total}]\}$ during deprotonation.

4a). A set of parallel lines is drawn according to Nernst's eq 7 where values of x are evenly distributed from 0.33 to 1. Stoichiometric $GR(CO_3^{2-})$ is below and fully ferric $GR(CO_3^{2-})^*$ above these lines. Lines for various redox reactions are also displayed for a few pollutants where activities are set equal (*15*).

These pollutants could be reduced in situ by $GR^*(x)$ while increasing slightly the ferric ratio within the $[(1/3)-(2/3)]$ range, that of fougerite. Lines (a) and (b) prove that nitrate can be reduced into nitrite and ammonium whatever the pH and line (c) into dichromate in acidic conditions only.

Domains of existence of various $GR^*(x)$ with regard to oxidation into α-FeOOH or formation from $Fe(OH)_2$ (Figure 4b) explain with the insert the shape of the domains around triple points T where equilibrium among three phases exists (*26*). The dotted line corresponds to equilibrium between $Fe(OH)_2$ and α-FeOOH, i.e., half-reaction by reduction is

$$\alpha\text{-FeOOH} + H^+ + e^- \rightarrow Fe(OH)_2 \text{ and}$$
$$E_h = 0.121 - 0.0591\text{pH} \quad (12)$$

Triple point T on the dotted line migrates toward acidic conditions when x increases. Points T_1, T_2, and T_3 are displayed for respective values of $x = 0.33$, 0.42, 0.50 giving respective pH of 12.3, 11, and 7.5. For the two first x values, the major soluble anion is CO_3^{2-}, whereas for $x = 0.50$, the most frequent value observed in the field for fougerite, HCO_3^- is in the majority in circumneutral conditions.

Fougerite Identification. Fougerite formation comes from bioreduction of ferric oxyhydroxides as proved in the laboratory (*27*). Bacteria trapped in an anoxic aquifer, e.g., DIRB, replace oxygen by Fe^{III} as electron acceptor and ferric oxyhydroxides dissolve gradually into Fe^{II} ions. Bacteria produce concomitantly HCO_3^- ions, and all constituents are present to produce Fe^{II-III} oxyhydroxycarbonate, i.e.:

$$6xFe^{III}OOH + 6(1-x)Fe^{2+} + HCO_3^- + 12(1-x)H_2O \rightarrow$$
$$Fe_6O_{12}H_{2(7-3x)}CO_3 + (11-12x)H^+ \quad (13)$$

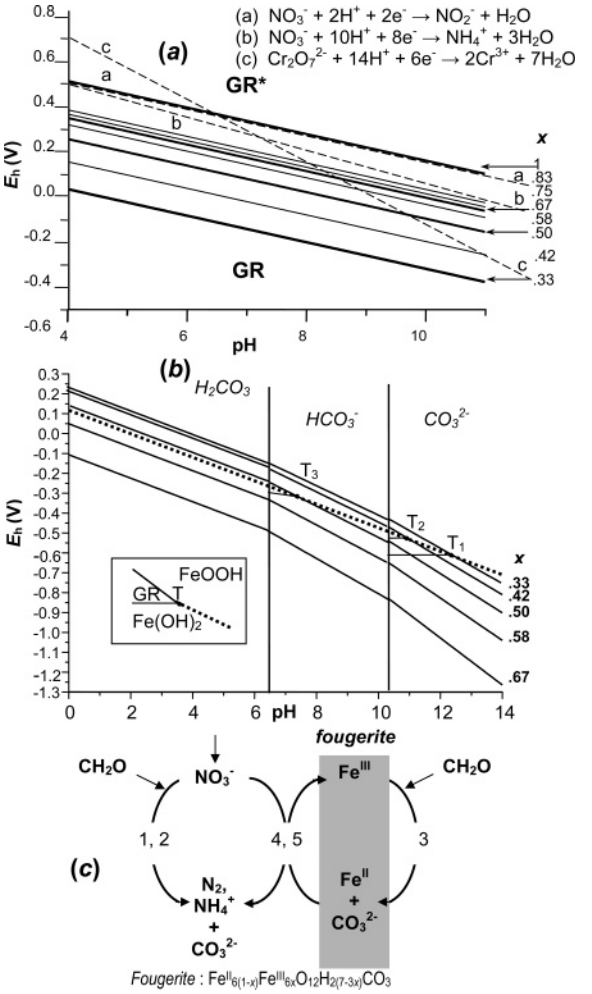

FIGURE 4. E_h−pH diagrams of the Fe^{II-III} (oxy)hydroxycarbonate (a) equilibrium lines of $GR^*(x)$ during deprotonation of $GR^*(x)$ as function of $x = \{[Fe^{III}]/[Fe_{total}]\} \in [(1/3)-1]$ and reduction reactions of some pollutants (equimolar activities) allowing prediction of the potential of fougerite to reduce them in the field; (b) domains of $GR^*(x)$ with $Fe(OH)_2$ and α-FeOOH for $x \in [(1/3)-(2/3)]$; (c) Fe−N cycles coupling in anoxic soils with fougerite acting as electron shuttle; organotrophic NO_3^- reduction to N_2 (1) or NH_4^+ (2); organotrophic dissimilatory Fe^{III} reduction (3); lithotrophic [Fe^{II}-driven] NO_3^- reduction to N_2 (4) or to NH_4^+ (5) [interpreted from ref *33*].

Reduction of γ-FeOOH by *Shewanella putrefaciens* yielded large crystals (∼5 μm diameter) of well characterized $GR(CO_3^{2-})^*$ and the reduction rate was evaluated by Mössbauer spectroscopy (*27*). Quadrupole doublets D_1, D_2, and D'_3 (D_3 and D_4 are not resolved) belong to $GR(CO_3^{2-})^*$ and D_γ due to remaining γ-FeOOH decreases from 100% to 35 and 15% during bioreduction from 1 to 6 days (Figure 5a) (*27*). The ratio x of $GR(CO_3^{2-})^*$ produced by bioreduction is about 0.50.

Figure 5b displays the first spectrum when fougerite was claimed to be a GR (*10−12*) whereas Figure 5c displays that of controlled $GR(CO_3^{2-})^*$ with $x = 0.50$. For the first time, a sample prepared chemically in the laboratory presents a Mössbauer spectrum identical to that found for a natural sample, establishing that the chemical counterpart of fougerite is clearly Fe^{II-III} oxyhydroxycarbonate $GR(CO_3^{2-})^*$. All occurrences of the mineral in the field show that ratio x is limited to the range $[(1/3)-(2/3)]$ (*6, 11, 12, 21, 22*).

Coupling of Iron and Nitrogen Cycles. Fe^{II} ions within solution can reduce many pollutants (*28*), e.g., nitrate, selenate, chromate, aromatics, etc. Among all possible

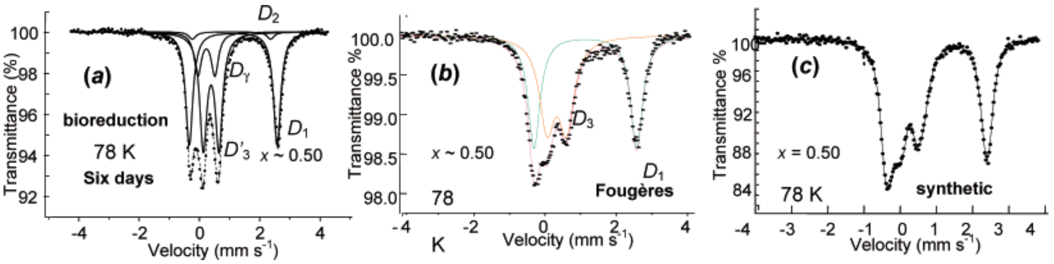

FIGURE 5. Mössbauer spectra measured at 78 K of GR(CO_3^{2-})* prepared in the lab and extracted from the field. (a) GR(CO_3^{2-})* obtained after 6 days by bioreduction of γ-FeOOH with *Shewanella putrefaciens* (*27*), (b) fougerite (*11, 12*), and (c) synthetic GR(CO_3^{2-})*.

reservoirs of Fe^{II} in Nature, fougerite is unique since bacterial activity may adjust its redox potential without changing the crystal structure. Therefore, occurrences exist in which the amount of fougerite is sufficient for soil remediation, the way synthetic GRs reduce all these pollutants (*29*−*32*). Taking the example of nitrate, the reaction is

$$Fe^{II}{}_4Fe^{III}{}_2(OH)_{12}CO_3 + (3/8)NO_3^- + (7/4)H^+ \rightarrow$$
$$5Fe^{III}OOH + HCO_3^- + Fe^{2+}{}_{aq} + (25/8)H_2O + (3/8)NH_4^+ \tag{14}$$

Three Fe^{II} ions out of four are oxidized whereas one is released into solution; thus the reaction can proceed where $Fe^{2+}{}_{aq}$ can ultimately be incorporated into lepidocrocite in acidic conditions or into ferrihydrite in a buffered medium (*19*).

Cycles of iron and nitrogen are obviously coupled. Oxidation of GR(CO_3^{2-})* by NO_3^- is continuous by in situ deprotonation, and a feedback between oxidation by nitrate and reduction by, e.g., DIRB fixes the value of x within reacting GR*. Both dissimilatory Fe^{III} reduction and oxidation of Fe^{II} with reduction of NO_3^- to NH_4^+ have been recently documented (*33*) and the potential Fe−N redox pathways in anoxic sediments must be completed by inserting fougerite, which is the solid-state redox mediator acting as electron shuttle, a feature unique among Fe-bearing minerals that allows enhancing the efficiency of nitrate-reducing organisms (Figure 4c). Finally, although NH_4^+ is obtained in the laboratory (*29*), it likely becomes N_2 in soils where NH_4^+ is unstable in sediments where anaerobic ammonium is oxidized by specific bacteria in anoxic water columns (anammox) (*34*).

Remediation of Waterlogged Soils. High concentrations of nitrate observed in agricultural areas are usually diffuse and scattered requiring the complete treatment of a given river basin. Configurations exist where sediments made of clay minerals mixed with fougerite (*22*) are viable for a natural purification because of their abundance despite intense agricultural activity (*6, 7*). Thus, even though nitrate concentrations are high in the soil upper cover, its absence under the redox front is due to abiotic reduction by Fe^{II} in gleysol where organic matter and bacterial activity are orders of magnitude lower. A Mössbauer spectrum at 78 K of a sample extracted from the oxidized zone above the redox front displays two types of ferric components: (*i*) magnetically split sextets attributed to goethite and/or ferrihydrite with abundance of 32%, and (*ii*) paramagnetic doublets that might be attributed to ferric GR(CO_3^{2-})* (48%) with some Fe^{III} trapped within clayey till (10%) (Figure 17 of ref *22*).

In contrast, in places such as Brittany (France) where agriculture is also very intense, natural water purification is insufficient. No solution has been found yet for major disorders, such as the proliferation of algae *Ulva armoricana* (*35*) in the sea at river-mouths, and nitrate concentration is 30−40 mg L^{-1} in the bay of Lieue de Grèves (Côtes d'Armor) (*36*) whereas the trigger for algae proliferation is 8 mg L^{-1}. Any effort to decrease the amount of nitrate from livestock is worthwhile, but no significant decrease in nitrate content has been observed for the past 10 years. The remarkable in situ redox flexibility of Fe^{II-III} oxyhydroxycarbonate can be used by mimicking what Nature does. A task of recovery is envisioned by treating the catchments of rivers, creating specific waterlogged areas with reinforced iron purification (WARIP) where the present soil would be replaced by a mixture of iron ore and organic compost to enhance fougerite formation. Finally, should the catalytic effect of iron that helps bacterial activity for reducing nitrate not be more specifically attributed to fougerite that acts as electron shuttle (Figure 4c)?

Acknowledgments

We thank M. Abdelmoula (LCPME-Nancy) for experimental help, A. Herbillon (Louvain la Neuve University) for discussions, the Region of Lorraine (C.U. and A.G.) and French Department of Education (G.O.) for support, and reviewers for their comments.

Literature Cited

(1) Hiscock, K. M.; Lyoyd, J. W.; Lerner, D. N. Review of natural and artificial denitrification of groundwater. *Water Res.* **1991**, *25*, 1099−1111.
(2) Korom, S. F. Natural denitrification in the saturated zone: a review. *Water Resour. Res.* **1992**, *28*, 1657−1668.
(3) Zeng, R. J.; Yuan, Z.; Keller, J. Improved understanding of the interactions and complexities of biological nitrogen and phosphorus removal processes. *Rev. Environ. Sci. Bio/Technol.* **2004**, *3*, 265−272.
(4) Van de Pas-Schoonen, K. T.; Schalk-Otte, S.; Haaijer, S.; Schmid, M.; Op den Camp, H.; Strous, M.; Gijs Kuenen, J.; Jetten, M. S. M. Complete conversion of nitrate into dinitrogen gas in cocultures of denitrifying bacteria. *Biochem. Soc. Trans.* **2005**, *33*, 205−209.
(5) Lind, A. M.; Pedersen, M. B. Nitrate reduction in the subsoils. II. General description of boring profiles, and chemical investigations on the profile cores. *Danish J. Plant Soil Sci.* **1976**, *80*, 82−99.
(6) Ernstsen, V. Reduction of nitrate by Fe^{2+} in clay minerals. *Clays Clay Miner.* **1996**, *44*, 599−608.
(7) Ernstsen, V.; Mørup, S. Nitrate reduction in clayey till by Fe(II) in clay minerals. *Hyperfine Interact.* **1992**, *70*, 1001−1004.
(8) Taylor, R. M. Colour in soils and sediments − A review. *Dev. Sedimentol.* **1982**, 749−761.
(9) Vysostsky, G. N. Gley. *Eurasian Soil Sci. (Pochvovedenie)* **1905**, *4*, 291−327.
(10) Trolard, F.; Abdelmoula, M.; Bourrié, G.; Humbert, B.; Génin, J.-M. R. Mise en évidence d'un constituant de type rouille verte dans les sols hydromorphes − Proposition de l'existence d'un nouveau minéral: la fougérite. *C. R. Acad. Sci., Paris* **1996**, *323-IIa*, 1015−1022.
(11) Trolard, F.; Génin, J.-M. R.; Abdelmoula, M.; Bourrié, G.; Humbert, B.; Herbillon, A. J. Identification of a green rust mineral in a reductomorphic soil by Mössbauer and Raman spectroscopies. *Geochim. Cosmochim. Acta* **1997**, *61*, 1107−1111.
(12) Génin, J.-M. R.; Bourrié, G.; Trolard, F.; Abdelmoula, M.; Jaffrezic, A.; Refait, Ph.; Maître, V.; Humbert, B.; Herbillon, A. J.

Thermodynamic equilibria in aqueous suspensions of synthetic and natural Fe(II)−Fe(III) green rusts: Occurrences of the mineral in hydromorphic soils. *Environ. Sci. Technol.* **1998**, *32*, 1058−1068.
(13) Bernal, J. D.; Dasgupta, D. R.; Mackay, A. L. The oxides and hydroxides of iron and their structural interrelations. *Clay Miner. Bull.* **1959**, *4*, 15−30.
(14) Ponnamperuma, F. N.; Tianco, E. M.; Loy, T. Redox equilibria in flooded soils. I. The iron hydroxide system. *Soil Sci.* **1967**, *103*, 374−382.
(15) Génin, J.-M. R.; Refait, Ph.; Bourrié, G.; Abdelmoula, M.; Trolard, F. Structure and stability of the Fe(II)-Fe(III) green rust “fougerite” mineral and its potential for reducing pollutants in soil solutions. *Appl. Geochem.* **2001**, *16*, 559−570.
(16) Vucelic, M.; Jones, W.; Moggridge, G. D. Cation ordering in synthetic layered double hydroxides. *Clays Clay Miner.* **1997**, *45*, 803−813.
(17) Génin, J.-M. R.; Olowe, A. A.; Refait, Ph.; Simon, L. On the stoichiometry and Pourbaix diagram of Fe(II)-Fe(III) hydroxysulphate or sulphate-containing green rust 2: An electrochemical and Mössbauer spectroscopy study. *Corros. Sci.* **1996**, *38*, 1751−1762.
(18) Refait, Ph.; Abdelmoula, M.; Génin, J.-M. R. Mechanisms of formation and structure of green rust one in aqueous corrosion of iron in the presence of chloride ions. *Corros. Sci.* **1998**, *40*, 1547−1560.
(19) Benali, O.; Abdelmoula, M.; Refait, Ph.; Génin, J.-M. R. Effect of orthophosphate on the oxidation products of Fe(II)-Fe(III) hydroxycarbonate: the transformation of green rust to ferrihydrite. *Geochim. Cosmochim. Acta* **2001**, *65*, 1715−1726.
(20) Hansen, H. C. B. Environmental chemistry of iron(II)-iron(III) LDHs. In *Layered Double Hydroxides*; Rives, V., Ed.; Nova Sci. Publ.: Huntington, 2001; pp 413−434 .
(21) Féder, F.; Trolard, F.; Klingelhöfer, G.; Bourrié, G. In situ Mössbauer spectroscopy: Evidence for green rust (fougerite) in a gleysol and its mineralogical transformations with time and depth. *Geochim. Cosmochim. Acta* **2005**, *69*, 4463−4483.
(22) Génin, J.-M. R.; Aissa, R.; Géhin, A.; Abdelmoula, M.; Benali, O.; Ernstsen, V.; Ona-Nguema, G.; Upadhyay, C.; Ruby, C. Fougerite and Fe^{II-III} hydroxi-carbonate green rust; ordering, deprotonation and/or cation substitution; structure of hydrotalcite-like compounds and mythic ferrosic hydroxide $Fe(OH)_{(2+x)}$. *Solid State Sci.* **2005**, *7*, 545−572.
(23) Ruby, C.; Géhin, A.; Abdelmoula, M.; Génin, J.-M. R.; Jolivet, J.-P. Coprecipitation of Fe(II) and Fe(III) cations in sulphated aqueous medium and formation of hydroxisulphate green rust. *Solid State Sci.* **2004**, *5*, 1055−1062.
(24) Bocher, F.; Géhin, A.; Ruby, C.; Ghanbaja, J.; Abdelmoula, M.; Génin, J.-M. R. Coprecipitation of Fe(II−III) hydroxycarbonate green rust stabilised by phosphate adsorption, *Solid State Sci.* **2004**, *6*, 117−124.
(25) Legrand, L.; Mazerolles, L.; Chaussé, A. The oxidation of carbonate green rust into ferric phases: solid-state reaction or transformation via solution. *Geochim. Cosmochim. Acta* **2004**, *68*, 3497−3507.
(26) Drissi, S. H.; Refait, Ph.; Abdelmoula, M.; Génin, J.-M. R. Preparation and thermodynamic properties of Fe(II)-Fe(III) hydroxycarbonate (green rust 1), Pourbaix diagram of iron in carbonate-containing aqueous media. *Corros. Sci.* **1995**, *37*, 2025−2041.
(27) Ona-Nguema, G.; Abdelmoula, M.; Jorand, F.; Benali, O.; Géhin, A.; Block, J.-C.; Génin J.-M. R. Iron(II,III) hydroxycarbonate green rust formation and stabilization from lepidocrocite bioreduction. *Environ. Sci. Technol.* **2002**, *36*, 16−20.
(28) Hardelein, S. B.; Pecher, K. Pollutant reduction in heterogeneous Fe(II)−Fe(III) systems. *ACS Symp. Ser.* **1998**, *715* (Mineral−Water Interfacial Reactions), 342−357.
(29) Hansen, H. C. B.; Koch, C. B. Reduction of nitrate to ammonium by sulfate green rust: activation energy and reaction mechanism. *Clay Miner.* **1998**, *33*, 87−101.
(30) Loyaux-Lawniczak, S.; Refait, Ph.; Ehrhardt, J.-J.; Lecomte, P.; Génin, J.-M. R. Trapping of Cr by formation of ferrihydrite during the reduction of chromate ions by Fe(II)−Fe(III) hydroxisalt green rusts. *Environ. Sci. Technol.* **2000**, *34*, 438−443.
(31) Myneni, S. C. B.; Tokunaga, T. K.; Brown, G. E., Jr. Abiotic selenium redox transformations in the presence of Fe(II,III) oxides. *Science* **1997**, *278*, 1106−1109.
(32) Refait, Ph.; Simon, L.; Génin, J.-M. R. Reduction of SeO_4^{2-} anions and anoxic formation of iron(II)−iron (III) hydroxi-selenate green rust. *Environ. Sci. Technol.* **2000**, *34*, 819−825.
(33) Weber K. A.; Urrutia M. M.; Churchill P. F.; Kukkadapu R. K.; Roden E. E. Anaerobic redox cycling of iron by freshwater sediment microorganisms. *Environ. Microbiol.* **2006**, *8*, 100−113.
(34) Dalsgaard, T.; Thamdrup, B.; Canfield, D. E. Anaerobic ammonium oxidation (anammox) in the marine environment. *Res. Microbiol.* **2005**, *156*, 457−464.
(35) Dion, P.; Reviers, B. D.; Coat, G. *Ulva armoricana* sp. nov. (Ulvales, Clorophyta) from the coasts of Brittany (France). I. Morphological identification. *Eur. J. Phycol.* **1998**, *33*, 73−80.
(36) Tanguy, H.; Lidou, F. La lutte préventive contre la prolifération des algues vertes: démarche engagée en baie de Saint-Michel-en-Grève. In *Pollutions Diffuses: du Bassin Versant au Littoral (Nonpoint Source Pollutions: from Watershed to Sea Shore)*; Merceron, M., Ed.; Ifremer: Plouzané, France, 1999; pp 261−275.

Received for review March 22, 2006. Revised manuscript received May 26, 2006. Accepted May 30, 2006.

ES0606834